Optics Letters

Retrieval of weak x-ray scattering using edge illumination

Charlotte J. Maughan Jones,[1,*] Fabio A. Vittoria,[1] Alessandro Olivo,[1] Marco Endrizzi,[1] and Peter R. T. Munro[1,2]

[1]Department of Medical Physics and Biomedical Engineering, Malet Place Engineering Building, University College London, WC1E 6BT, UK
[2]School of Electrical, Electronic and Computer Engineering, The University of Western Australia, 35 Stirling Highway, Perth, WA 6009, Australia
*Corresponding author: rmapmau@ucl.ac.uk

Received 10 April 2018; revised 21 May 2018; accepted 24 May 2018; posted 5 June 2018 (Doc. ID 327895); published 6 August 2018

X-ray phase contrast imaging provides additional modes of image contrast compared to conventional attenuation-based x-ray imaging, thus providing additional structural and functional information about the sample. The edge-illumination (EI) technique has been used to provide attenuation, refraction, and scattering contrast in both biological and non-biological samples. However, the retrieval of low scattering signals by fitting a single Gaussian remains problematic, principally due to the inability of the EI system to achieve perfect dark-field illumination. We present a new retrieval method that fits three Gaussians, which successfully overcomes this limitation, and provide examples of the retrieval of such signals in highly absorbing, weakly scattering samples.

OCIS codes: (110.7440) X-ray imaging; (340.7440) X-ray imaging; (340.7430) X-ray coded apertures; (120.5820) Scattering measurements; (100.5070) Phase retrieval.

https://doi.org/10.1364/OL.43.003874

X-ray phase contrast imaging (XPCi) is an advanced, multimodal, x-ray imaging method that utilizes the phase shift or refraction induced by an object as an x-ray beam traverses it [1,2], as opposed to conventional x-ray imaging, in which contrast is solely reliant on x-ray attenuation. XPCi techniques offer increased contrast [1], as well as extra diagnostic information when the attenuation, refraction (or phase), and scattering contributions to signal are retrieved.

The edge-illumination (EI) technique, as depicted in Fig. 1(a), was initially developed for synchrotron sources [3], however was subsequently translated to polychromatic, non-microfocal, laboratory sources with divergent beams [4], demonstrating the technique's ability to operate under relaxed coherence requirements. The laboratory system consists of a set of two masks; the first (sample mask) is used to split the beam into a series of beamlets, and may be misaligned with respect to the second (detector mask), which is aligned with the detector pixels. The sample is introduced in between the two masks, and the signal is obtained when the beamlets are deflected either onto or away from the absorbing columns of the detector mask, creating negative and positive refraction signals, respectively. The illumination curve (IC) is unique to the system setup without a sample in place, and is obtained by incrementally scanning the sample mask through a series of sub-pixel-sized steps (sample mask positions) in relation to a static detector mask while recording the integrated intensity sensed by each pixel at each mask position [5].

The scattering signal contains complementary information about the microscopic, sub-pixel structure of samples, and is caused by refraction from such structures [6,7]. This is observed as a broadening of the beamlet created by the sample mask, and therefore also a broadening in the IC observed in each pixel [8,9]. Retrieval of the scattering signal has concentrated on tracking this broadening [8,10,11]; however, true dark-field imaging is an alternative, where the sample mask is completely misaligned with respect to the detector mask [3,12]. However, in practice, the beamlets are broadened by a combination of geometrical blurring by the focal spot and

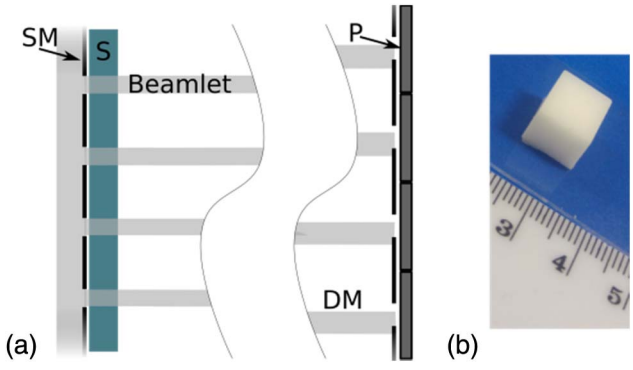

Fig. 1. (a) Edge illumination system, including sample mask (SM), sample (S), detector mask (D), and pixel (P). (b) Phantom of TiO_2 concentration 0.77%, mounted on a glass slide, ready for imaging.

partial transmission by the sample mask, which, combined with partial transmission of the detector mask, prevents the achievement of perfect dark-field illumination. This causes the IC extinction ratio, the ratio between the maximum and minimum IC values, to be finite. We note that while the masks are designed to be 98% absorbing at photon energy 40 keV, a lower absorption is achieved in practice [11], due either to underplating or to a reduced density of the plated material. Thus far, scattering retrieval has been restricted to samples with scattering properties unable to be tailored, such as paper [8,11], breast calcifications [8], composite materials [13], and alveolar tissues [14], all of which are weakly attenuating. Quantitative retrieval in highly attenuating and well-controlled weakly scattering samples has not been investigated.

In this study, we present a new retrieval method that can accurately and quantitatively determine the scattering signal from a system with a finite IC extinction ratio, using samples with a weak scattering signal. We discuss the problems of beam hardening in highly absorbing samples, and discuss two flat-fielding methods that overcome these problems. The applications to biological tissues are also theorized and briefly discussed.

Materials and Methods. Phantoms were constructed using TiO_2 powder with a mean particle size of <5 μm [Product 224227, Titanium(IV) oxide, rutile, Sigma Aldrich, Dorset, UK], embedded within a two-part room temperature vulcanizing silicone rubber (Elastosil RT 601 A/B, Wacker Chemie AG, Munich, Germany) as the bulk material. The silicone consists of a viscous, catalyst containing "part A," which, when mixed with "part B" and left at room temperature, cures to form a stable and solid silicone rubber [15]. It was initially chosen as a bulk material due to its high x-ray attenuation, with TiO_2 chosen as a suitable x-ray scatterer due to the difference in δ value between it and the silicone, approximately 9.2×10^{-7} and 2.5×10^{-7}, respectively, at 30 KeV, as well as the particle size being smaller than the pixel size of the detector. The phantoms were manufactured using a previously presented method [16]. Although this method was used to embed silica microspheres in silicone, it was found to also produce homogeneous scattering phantoms when the silica microspheres were replaced with TiO_2 powder; therefore, no modifications to the method were required. The silicone mixture was cast in a 1 cm^3 silicone ice cube mold that was sprayed with a non-silicone release agent (Ambersil Formula 5. CRC Industries UK Ltd., Somerset, UK) to facilitate the removal of the cured sample from the casts, creating cuboid phantoms of equal height, width, and depth [Fig. 1(b)]. These were then mounted on glass slides using epoxy resin to create physical stability during imaging. Phantoms of six different scatterer concentrations were created: 0.12%, 0.23%, 0.36%, 0.48%, 0.59%, and 0.77% scatterer by weight, along with a plain silicone phantom of the same dimensions. Scatterer by weight represents the initial mass of TiO_2 in comparison to the initial mass of silicone part A used.

Images were acquired using the previously described EI system [8], with a Mo source operated at 40 kV and 30 mA, along with a Pixirad (Pixirad Imaging Counters s.r.l., Italy) photon-counting detector with pixel size of 62×62 μm^2. The masks were manufactured by Creatv MicroTech (Potomac, Maryland). The sample and detector masks had a pitch of 48 μm and 59 μm, and aperture width of 12 μm and 17 μm, respectively. The source to detector distance was 1.26 m, and the sample and detector masks were placed so that the magnified periods of both masks were equal to the pixel size of the detector, at 0.98 m and 1.20 m from the source, respectively. The IC was generated using 15 sample mask positions with subsequent flat-field and object images acquired using 33 sample mask positions distributed symmetrically about mask position 17, the point of maximum pixel exposure. The flat-field image was either an:

1. Image in the absence of a sample (standard flat field), or
2. image in the presence of plain silicone—homogenous, assumed non-scattering sample (alternative flat field),

with the second approach being used to negate the beam hardening effect of the high-attenuation phantoms. The object image is obtained with the same system parameters as the flat field except for the presence of the scattering phantom. The exposure time for the IC and flat-field and object images at each mask position was 250 ms so as to eliminate the possibility of pixel saturation, and a total of 16 frames per mask position were taken. For analysis, all 16 frames per sample mask position were summed so as to improve the signal-to-noise ratio.

A new method of retrieval for quantitative determination of very weak x-ray scattering signal was developed to overcome the problems caused by a finite IC extinction ratio, which were encountered using previously described methods [8,11]. Previous retrieval methods consider a single, independent, Gaussian per pixel to represent the IC before the introduction of a sample, which is reduced in amplitude, shifted along the direction perpendicular to the mask apertures, and broadened by attenuation, refraction, and scattering effects of the sample, respectively [8]. The following retrieval method (three Gaussian retrieval) accounts for the fact that adjacent pixels are not independent of one another.

Signal retrieval was performed on the same 81×13 pixel area of each image where the phantom was present. The same pixels were used for the IC, object, and flat-field image for each scatterer concentration. Three overlapping Gaussians separated by the sample mask period of 48 μm were fitted to the illumination curve data, as illustrated in Fig. 2, from three horizontally adjacent and non-independent pixels to gain the coefficients a_i, b_i, and c_i, unique to each set of three pixels:

$$y_{\mathrm{IC}}(x) = \sum_{i=-1}^{1} a_i \frac{e^{\left(\frac{-(x-b_i+i\Delta)^2}{2c_i^2}\right)}}{\sqrt{2\pi(c_i^2)}}, \tag{1}$$

where y_{IC} is the recorded number of counts at each sample mask position, $\Delta = 0.048$ mm (sample mask period), and x is the sample mask position in mm. The fitting process continues, moving one pixel in the horizontal direction until each group of three horizontally adjacent pixels are assigned nine coefficients in total. Only the three coefficients corresponding to the central pixel are retained to contribute to the retrieved image.

Three overlapping Gaussians separated by the sample mask period are subsequently fitted to the experimental data obtained when a sample is in place in the system. Utilizing the parameters gained from the illumination curve fitting, the values of t_i, r_i, and s_i are obtained:

$$y_{\mathrm{object}}(x) = \sum_{i=-1}^{1} t_i \left(a_i \frac{e^{\left(\frac{-(x-b_i-r_i+i\Delta)^2}{2(c_i^2+s_i)}\right)}}{\sqrt{2\pi(c_i^2+s_i)}} \right), \tag{2}$$

where y_{object} is the recorded number of counts at each sample mask position (x). The parameters t_i, r_i, and s_i (maxima, position of the maxima, and variance of the curve, respectively) are kept for the central pixel ($i = 0$) and discarded for the pixels on the left and right ($i = 1$ and $i = -1$), leaving one set of parameters (t_{object}, r_{object}, s_{object}) per pixel. This process [Eq. (2)] is repeated for the flat-field image to obtain a further set of parameters (t_{flat}, r_{flat}, s_{flat}) per pixel.

To obtain the final attenuation (t_{image}), refraction (r_{image}), and scattering (s_{image}) images, the following equations can be used on a pixel-by-pixel basis:

$$t_{image} = \frac{t_{object}}{t_{flat}}(\text{a.u.}), \tag{3}$$

$$r_{image} = r_{object} - r_{flat}(\text{mm}), \tag{4}$$

$$s_{image} = s_{object} - s_{flat}(\text{mm}^2). \tag{5}$$

This method can be used to retrieve the attenuation, refraction, and scattering signal from a sample; however, only the scattering signal shall be presented and discussed with respect to the phantoms described.

Results: To enable direct comparison between samples, the values of s_{image} were corrected by the background, so that all areas of the image without a sample present have a value of 0. The background value of s_{image} was calculated from the mean of a 76 × 13 pixel retrieved area where no sample was present, and this value was subtracted from every pixel within the image. The values of s_{image} presented were calculated from the mean of all the pixels in the retrieved area.

Figure 3 shows that if the standard flat-fielding method is used, the s_{image} values are negative; however, if the values are rigidly translated so that a phantom with 0% scatterer concentration (i.e., plain silicone) has a value of $s_{image} = 0$ mm^2, then

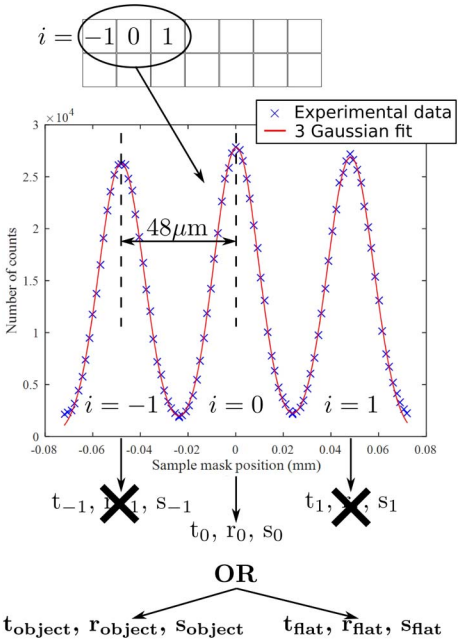

Fig. 2. Schematic of the "three Gaussian retrieval" on an image (7 × 2 pixels), including an example of the fit obtained using experimental data, to gain either the object or flat-field parameters (t, r, and s).

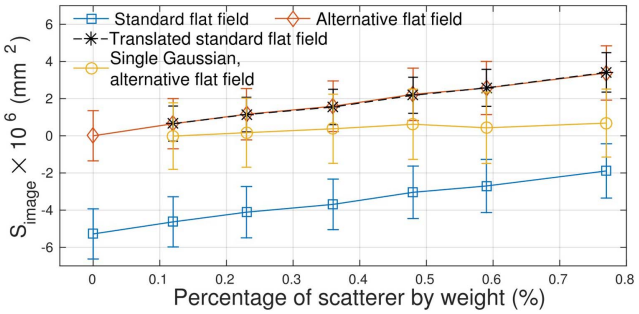

Fig. 3. s_{image} value calculated for each of the phantoms using both the standard flat-field image and the alternative flat-field image. The value of s_{image} calculated using the standard flat-field image, translated so that 0% scatterer by weight has $s_{image} = 0$ mm^2, is also displayed. Error bars are ±1 standard deviation.

not only do the values become positive, but they follow the trend seen when using the alternative flat-fielding method. Negative values arise as a result of beam hardening reducing the width of the IC. Figure 3 also shows the retrieved s_{image} when only a single Gaussian is used, which deviates significantly from what is expected.

If the number of positions of the sample mask is reduced from 33 to 3 for both the object and flat-field images, to make the imaging acquisition protocol similar to those already described [11], then although the noise increases, the mean values of s_{image} remain relatively unchanged, and within the standard deviation of the original value (Fig. 4). We note that the uncertainty in the averaged data points plotted in Figs. 3 and 4 should be divided by $\sqrt{81 \times 13 - 1}$ according to the central limit theorem. This, however, results in an unreasonably low uncertainty due to systematic variations between pixels. We have thus opted to use only the standard deviation of retrieved values of S_{image} to estimate the uncertainty. The same can be observed regardless of whether the standard or alternative flat-fielding method was used. The three points used in these calculations corresponded to maximum pixel illumination (center of the IC) and to approximately 50% pixel illumination of either side of the IC (full width at half-maximum of IC).

Discussion. The detection of weak scattering signals in highly absorbing materials is made possible via the three Gaussian retrieval method presented, with a concentration of TiO_2 as low as 0.1% (% scatterer by weight) creating a small,

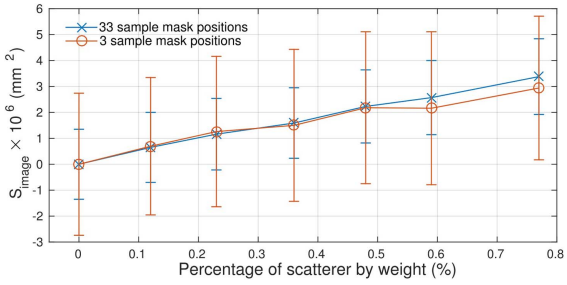

Fig. 4. Effect of reducing the number of sample mask positions of both the object and flat-field image to 3 from the original 33. Values displayed were obtained using the standard flat-field method then translated to 0.

but retrievable signal. This is akin to the relatively low x-ray scattering that would be expected from biological tissues, where the difference in delta is small between bulk material (e.g., extra cellular matrix) and the scatterers that reside within it (e.g., cells or cellular organelles). Previously reported scattering values for neoplastic breast tissues are approximately between 100 μrad^2, and 900 μrad^2, with calcifications demonstrating values above this [8] and the surrounding normal breast tissue demonstrating values of below 100 μrad^2 [8]. The samples considered in this study all demonstrate scattering below 100 μrad^2 and therefore can be considered similar to normal biological tissues. The reported three Gaussian fit works where the single Gaussian fit fails because the mismatch between the single Gaussian and the IC is more significant than the sample-induced change to the IC width. As the three Gaussian retrieval results in a substantially better fit to the IC, it accurately retrieves small-scale IC width changes.

The results in this Letter, made possible by the increased sensitivity of the three Gaussian fit, show that beam hardening and scattering both lead to changes in the width of the IC. While using phantoms, a non-scattering sample (plain silicone) is able to be manufactured alongside the scattering ones. This enables the translation of retrieved scattering values, for non-scattering samples, to 0 if standard flat fielding is performed, and facilitates the retrieval if alternative flat fielding is performed. Tissue is a heterogeneous material, and there are no biological tissues that could be considered as a non-scattering sample. To translate this method to biological tissues, a non-scattering and non-biological test material of approximately similar elemental composition and attenuation to the tissue of interest could be used, e.g., tissue equivalent plastics, or polymethyl methacrylat (PMMA) [17]—both of which have been used as tissue-mimicking x-ray phantom materials [18]. Alternatively, if absolute values of scattering are not required, and relative scattering between different tissue types in a field of view is sufficient, then local scattering contrast could be obtained, by comparing the signal from regions of a sample with similar thicknesses. Such approaches may lead to reduced sensitivity to scattering; however, we anticipate the three Gaussian retrieval to remain superior to the single Gaussian.

For translation into the biomedical field, close attention to the dose received by the patient is required. In previous scattering retrieval methods using edge illumination, three sample mask positions have been used [8,11,13,19]. It has been demonstrated that this new retrieval method has the ability to retrieve the scattering signal from three such sample mask positions per pixel, without losing significant accuracy. The limitation of reducing the number of sample mask positions per pixel appears to be the noise level, which increases, but the mean remains stable, which is important when quantitative retrieval is required.

Conclusion. Retrieval of weak scattering signals poses significant problems for EI systems with a finite IC extinction ratio. The new three Gaussian retrieval method is able to overcome this limitation allowing for the retrieval of weak scattering signals from highly absorbing materials. Use of this method could allow the retrieval of scattering in a range of biological tissues, which has the potential to provide complimentary diagnostic data alongside traditional attenuation radiography.

Funding. Engineering and Physical Sciences Research Council (EPSRC) (EP/M507970/1, EP/P005209/1); Royal Society (UF130304); Royal Academy of Engineering.

Acknowledgment. C. J. M. J. is supported by an EPSRC studentship. F. A. V. is supported by the Royal Academy of Engineering and the Office of the Chief Science Adviser for National Security under the UK Intelligence Community Postdoctoral Fellowship Programme. M. E. was supported by the Royal Academy of Engineering under the RAEng Research Fellowships scheme. P. R. T. M. is supported by a Royal Society University Research Fellowship.

REFERENCES

1. A. Olivo and E. Castelli, Riv. del Nuovo Cimento **37**, 467 (2014).
2. A. Bravin, P. Coan, and P. Suortti, Phys. Med. Biol. **58**, R1 (2013).
3. A. Olivo, F. Arfelli, G. Cantatore, R. Longo, R. H. Menk, S. Pani, M. Prest, P. Poropat, L. Rigon, G. Tromba, E. Vallazza, and E. Castelli, Med. Phys. **28**, 1610 (2001).
4. A. Olivo and R. Speller, Appl. Phys. Lett. **91**, 074106 (2007).
5. P. R. T. Munro, C. K. Hagen, M. B. Szafraniec, and A. Olivo, Opt. Express **21**, 11187 (2013).
6. F. Pfeiffer, M. Bech, O. Bunk, P. Kraft, E. F. Eikenberry, C. Brönnimann, C. Grünzweig, and C. David, Nat. Methods **7**, 134 (2008).
7. L. Rigon, H.-J. Besch, F. Arfelli, R.-H. Menk, G. Heitner, and H. Plothow-Besch, J. Phys. D **36**, A107 (2003).
8. M. Endrizzi, P. C. Diemoz, T. P. Millard, J. Louise Jones, R. D. Speller, I. K. Robinson, and A. Olivo, Appl. Phys. Lett. **104**, 024106 (2014).
9. M. Endrizzi, F. A. Vittoria, L. Rigon, D. Dreossi, F. Iacoviello, P. R. Shearing, and A. Olivo, Phys. Rev. Lett. **118**, 1 (2017).
10. F. A. Vittoria, G. K. N. Kallon, D. Basta, P. C. Diemoz, I. K. Robinson, A. Olivo, and M. Endrizzi, Appl. Phys. Lett. **106**, 224102 (2015).
11. M. Endrizzi and A. Olivo, J. Phys. D **47**, 505102 (2014).
12. A. Olivo, F. Arfelli, D. Dreossi, R. Longo, R. H. Menk, S. Pani, P. Poropat, L. Rigon, F. Zanconati, and E. Castelli, Phys. Med. Biol. **47**, 469 (2002).
13. M. Endrizzi, B. I. S. Murat, P. Fromme, and A. Olivo, Compos. Struct. **134**, 895 (2015).
14. P. Modregger, T. P. Cremona, C. Benarafa, J. C. Schittny, A. Olivo, and M. Endrizzi, Sci. Rep. **6**, 1 (2016).
15. Wacker Chemie AG, "Technical data sheet for Elastosil® RT 601 A/B," 2014, https://www.wacker.com/cms/en/products/product/product.jsp?product=10461.
16. C. J. Maughan Jones and P. R. T. Munro, J. Biomed. Opt. **22**, 1 (2017).
17. J. Hubbel and S. M. Seltzer, "Tables of x-ray mass attenuation coefficients and mass energy-absorption coefficients (Version 1.4)," National Institute of Standards and Technology, https://www.nist.gov/pml/x-ray-mass-attenuation-coefficients.
18. M. E. Poletti, O. D. Goncalves, and I. Mazzaro, Phys. Med. Biol. **47**, 47 (2002).
19. M. Endrizzi, D. Basta, and A. Olivo, Appl. Phys. Lett. **107**, 124103 (2015).